Journal of Korean Powder Metallurgy Institute
Vol. 16, No. 1, 2009

The Formation and Crystallization of Amorphous $Ti_{50}Cu_{20}Ni_{20}Al_{10}$ Powder Prepared by High-Energy Ball Milling

Nguyen Hoang Viet, Jin Chun Kim*, Ji Soon Kim and Young Soon Kwon
Research Center for Machine Parts and Materials Processing, School of Materials Science and Engineering, University of Ulsan, Daehakno 102, Ulsan 680-749, Korea
(Received December 18, 2008; Received in revised form January 19, 2009; Accepted January 29, 2009)

Abstract Amorphization and crystallization behaviors of $Ti_{50}Cu_{20}Ni_{20}Al_{10}$ powders during high-energy ball milling and subsequent heat treatment were studied. Full amorphization obtained after milling for 30 h was confirmed by X-ray diffraction and transmission electron microscope. The morphology of powders prepared using different milling times was observed by field-emission scanning electron microscope. The powders developed a fine, layered, homogeneous structure with prolonged milling. The crystallization behavior showed that the glass transition, T_g, onset crystallization, T_x, and super cooled liquid range $\Delta T = T_x - T_g$ were 691, 771 and 80 K, respectively. The isothermal transformation kinetics was analyzed by the John-Mehn-Avrami equation. The Avrami exponent was close to 2.5, which corresponds to the transformation process with a diffusion-controlled type at nearly constant nucleation rate. The activation energy of crystallization for the alloy in the isothermal annealing process calculated using an Arrhenius plot was 345 kJ/mol.

Keywords : Amorphous metal powder, Ti-Cu-Ni-Al, Mechanical alloying, Crystallization kinetic

1. Introduction

Bulk amorphous alloys with a wide supercooled liquid region (SLR) have been synthesized successfully in Zr-, Ln-, Fe-, Co-, Ni-, Cu-, Pd-, and Mg-based alloy system [1]. Ti-Based bulky amorphous alloy systems, such as Ti-Cu-Ni [2], Ti-Ni-Cu-Al [3], Ti-Zr-Ni-Cu-Al [4], Ti-Ni-Cu-Sn [5,6], and Ti-Ni-Cu-Si-B [7] have also been investigated due to their relatively lower density and/or higher specific strength. Inoue *et al.* [3, 8] reported that the extremely large glass-forming ability in Zr-Cu-Ni-Al and Ti-Cu-Ni-Al are presumably contributed by a combination of significantly different atomic size ratios among constituent elements and the necessity of redistribution of Al for the progress of crystallization. Therefore, it is expected that the possible increasing of SLR for Ti-based amorphous alloys can be expanded by using amorphous alloy system mainly consisting of Ti-based and Al element.

Mechanical alloying can be used to prepare amorphous alloys [9-10]. The as-milled powder alloys are suitable for further processing to fabricate bulk amorphous alloys; for example, bulk amorphous $Ti_{50}Cu_{25}Ni_{20}Sn_5$ [11] and $Al_{82}La_{10}Ni_4Fe_4$ [12] alloys were consolidated by spark-plasma sintering of mechanically alloyed Ti-Cu-Ni-Sn and Al-La-Ni-Fe powders, respectively. Furthermore, the properties of materials are usually determined by their microstructures, i.e., the nature, perfection, and spatial distribution of their component phase [13]. If one wants to control the morphology of precipates in amorphous matrix, it should be of significance to understand mechanism by which the crystallization happens in different bulk amorphous alloys.

In the present work, the amorphization and crystallization kinetics of the mechanically alloyed $Ti_{50}Cu_{20}Ni_{20}Al_{10}$ powder were investigated. Filed-emis-

*Corresponding Author : [Tel : +82-55-280-3573; E-mail : jckimpml@ulsan.ac.kr]

sion scanning electron microscope (FE-SEM) and X-ray diffraction (XRD) were used for morphology and structure characterization of powder alloy during MA. Differential scanning calorimetry (DSC) was used to evaluate the major temperatures and kinetic parameters relating to the crystallization process.

2. Experimental

Elemental powders of Ti, Cu, Ni, and Al with purities greater than 99% were accurately weighed and mixed in proportion to the atomic composition of $Ti_{50}Cu_{20}Ni_{20}Al_{10}$. MA was performed using an AGO-2 planetary ball mill with a speed of 300 rpm. Hardened steel vials and balls were used, and the ball-to-powder ratio was about 20:1 by weight. The vials were evacuated and filled with 5×10^3 Pa Ar gas to avoid oxidation of the powder particles. During milling, the vial was cooled by water in order to prevent an increase in temperature. The MA process was carried out using selected durations of 1, 2, 5, 10, 20, and 30 h; each MA process was performed without interruptions. X-ray diffraction (XRD) using Cu-K_α radiation was used for analysis of phase formation of the milled powder samples. Morphology of the mechanically-alloyed powder samples was analyzed by a field emission scanning electron microscopy (FE-SEM; JEOL JMS-6500F). Thermal properties of the as-milled amorphous powders were evaluated by differential scanning calorimetry (DSC) with a heating rate of 10 K/min under a continuous flow of Ar gas. For isothermal analysis, the amorphous alloys were first heated at rate of 80 K/min to a desired temperature within the SLR, and then the temperature was held for a certain period of time, until complete transformation was achieved.

3. Results and Discussion

The progress of amorphization during milling process was monitored by means of X-ray diffraction.

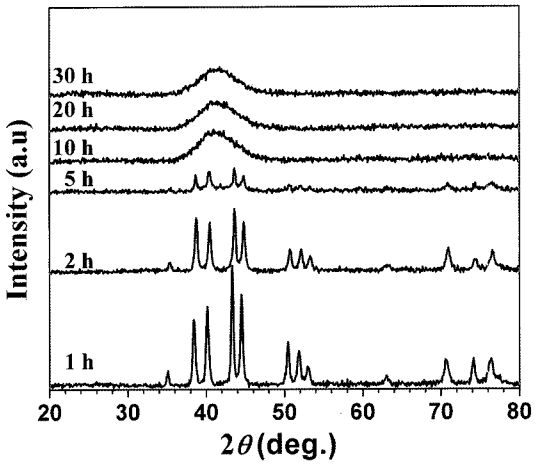

Fig. 1. XRD spectra of $Ti_{50}Cu_{20}Ni_{20}Al_{10}$ powder as function of milling time.

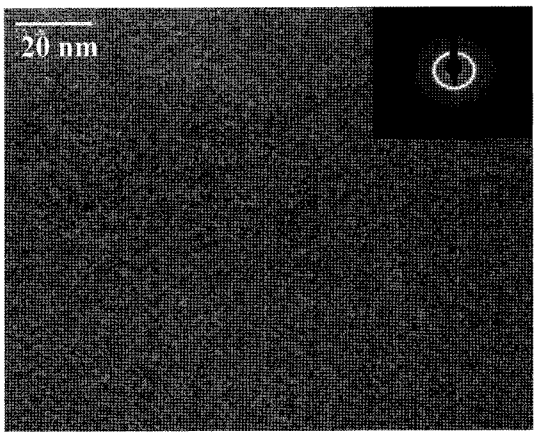

Fig. 2 HR-TEM micrograph (inset: selected area diffraction pattern) of the $Ti_{50}Cu_{20}Ni_{20}Al_{10}$ powder alloy milled for 30h.

The XRD spectra of $Ti_{50}Cu_{20}Ni_{20}Al_{10}$ powders after milling times ranging from 1 to 30 h are shown Fig. 1. Broad halo patterns which are typical in amorphous structure can be observed after milling time reached 30 h. No diffraction peaks of any crystalline metallic phases or oxides were appeared showing that a fully amorphous structure was formed.

The high-resolution transmission electron micrograph (HR-TEM) and the corresponding electron diffraction pattern of the $Ti_{50}Cu_{20}Ni_{20}Al_{10}$ powder alloy after milling for 30 h are given in Fig. 2. A selected area diffraction pattern (SADP) taken from

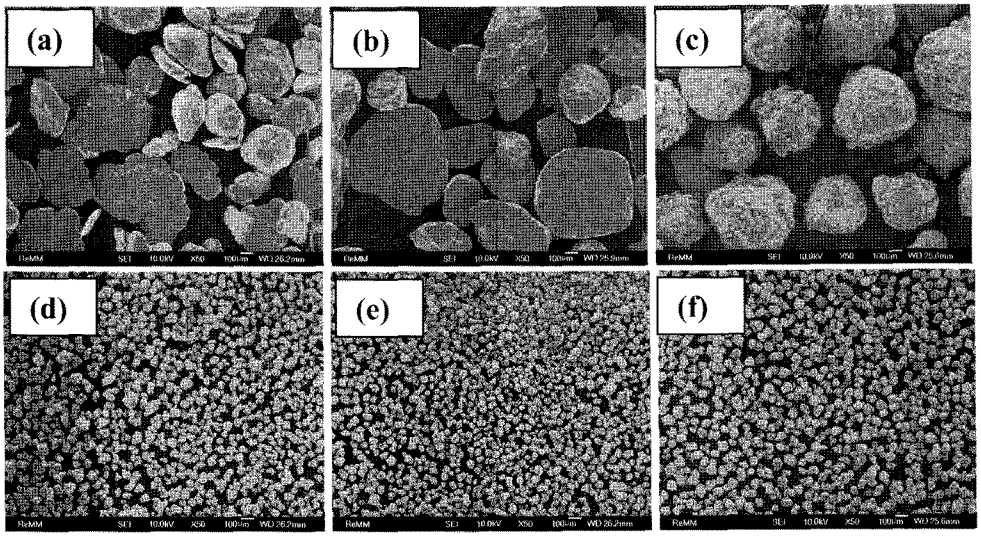

Fig. 3. FE-SEM images (X 50) of $Ti_{50}Cu_{20}Ni_{20}Al_{10}$ powder milled for (a) 1 h, (b) 2 h, (c) 5 h, (d) 10 h, (e) 20 h, and (f) 30 h.

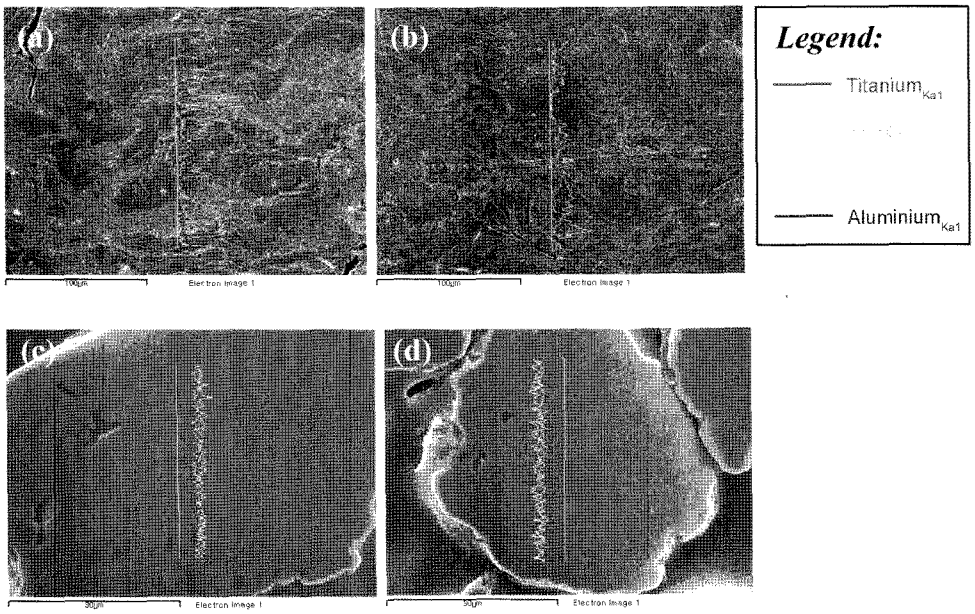

Fig. 4. FE-SEM/EDS profiles of the cross-sections of $Ti_{50}Cu_{20}Ni_{20}Al_{10}$ powder milled for (a) 2, (b) 5, (c) 10 and (d) 30 h.

this region shows a diffuse halo ring, indicating the amorphous structure of the alloy.

The morphology of the as-milled powders after different stages of the MA process was observed by FE-SEM (Fig. 3). After 1 and 2 h of milling the MA-processed powders showed different particles sticking over one another and particles were cold welded to form composite flatten-granules (Fig. 3(a-b)). The size of these granules was several hundreds of micrometers, and, in fact, the size of the granules increased initially with milling due to impact welding of particles. The shape of these granules changed drastically after 5 h of milling time (Fig 3(c)). Note that these granules have been fractured and mechani-

cally agglomerated to form large spherical particulates. For a milling time longer than 30 h, the large spherical particulates were formed into a fine spherical powder because of the fracturing process of MA (Fig. 2(d-f)). After 10 h of milling, changes in the size of the MA-processed powders become steady state, as shown in the XRD spectra.

Metallographical examinations of cross-sections of the powder after 2, 5, 10 and 30 h of milling are shown in Fig. 4. The spectrum lines in color express the distribution of metallic elements. Many intimate layers of elemental metals can be seen in the micrograph in Fig. 4(a-b). After milling for 10 h, the microstructure changed significantly and exhibited a fine structure (Fig. 4 c-d), indicating enhanced diffusion and a sufficient start to a solid state amorphizing reaction.

Fig. 5 presents the DSC scans of the amorphous $Ti_{50}Cu_{20}Ni_{20}Al_{10}$ alloy samples after 20 and 30 h of milling. The glass transition temperature, T_g, the onset temperature of primary crystallization, T_x and the crystallization enthalpy values for the amorphous $Ti_{50}Cu_{20}Ni_{20}Al_{10}$ as-milled powder are given in Table 1. The powder samples exhibited an endothermic, characteristic of the glass transition, followed by an SLR ($T_x = T_x - T_g$) and a peak resulting from primary crystallization. When the milling time

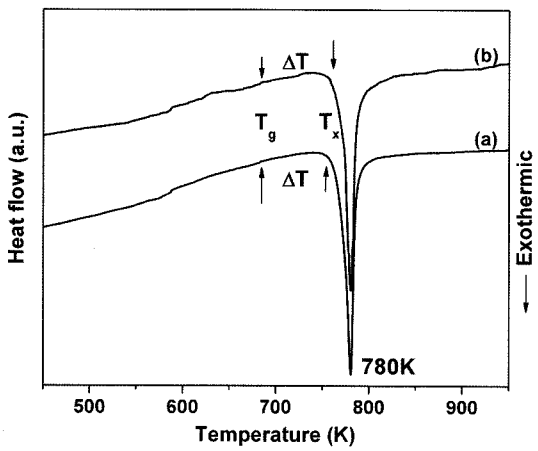

Fig. 5. DSC scans of $Ti_{50}Cu_{20}Ni_{20}Al_{10}$ powder milled for (a) 20 h and (b) 30 h.

Table 1. T_g, T_x, ΔT, and ΔH for $Ti_{50}Cu_{20}Ni_{20}Al_{10}$ as-milled powders with continuous heating at 10 K/min

Milling time h	T_g K	T_x K	ΔT K	ΔH J/g
20	691	766	75	85.89
30	691	771	80	85.68

was extended from 20 h to 30 h, T_g remained almost the same (T_g = 691 K), while the onset crystallization temperature (T_x) shifted from 766 K to 771 K, due to the accompanying change in the composition of the amorphous phase. The alloys exhibited large SLRs of 76 and 80 K (for 20 and 30 h, respectively), which means that the amorphous powder is beneficial for consolidation of bulk amorphous materials.

The isothermal thermograms of $Ti_{50}Cu_{20}Ni_{20}Al_{10}$ amorphous alloy MA-processed for 30 h and annealed at different temperatures in the range of the SLR were obtained and examined for behavior indicating transformation from amorphous to crystalline phase. The corresponding DSC curves are shown in Fig. 6a. Each DSC curve shows an incubation period followed by an exothermic peak, which corresponds to crystallization that is characteristic of amorphous materials. From the DSC curves, it is apparent that the incubation period decreased with increasing annealing temperature, indicating a typical nucleation and growth mode.

Fig. 6b presents the relationship between the crystallized volume fraction, x, and the annealing time, t. The value of x is proportional to the fractional area of the exothermic peak, so the crystallized volume fraction can be accurately determined by measuring the partial area of the exothermic signal. A typical sigmoidal-type curve for the crystallized volume fraction as a function of annealing time is obtained [14]. From the graph we can see that the crystallization process becomes faster as the annealing temperature increases.

The isothermal crystallization kinetics of amorphous alloys is normally described by the Johnson–

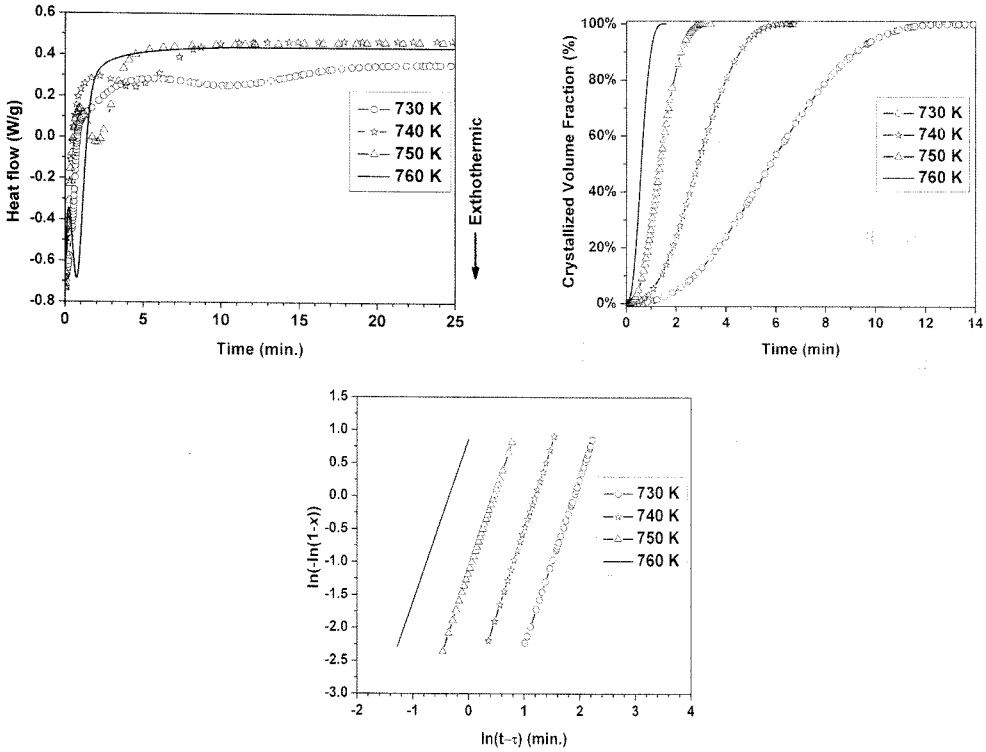

Fig. 6. (a) Isothermal curves, (b) crystallized volume fraction, x, as a function of time, t, and (c) JMA plots of amorphous $Ti_{50}Cu_{20}Ni_{20}Al_{10}$ alloy.

Mehl-Avrami (JMA) equation [15]:

$$x = 1 - e^{-[(t-\tau)]^n} \quad (1)$$

in which x is the transformed volume fraction (%), is the incubation time for the transformation taken as the time interval between the sample reaching the isothermal temperature and the initiation of the transformation, n is the Avrami exponent reflecting the characteristics of nucleation and growth during crystallization, and k is the reaction rate constant that is a function of annealing the temperature and assumed to be described by the Arrhenius equation:

$$k = k_0 e^{-\frac{E_c}{RT}} \quad (2)$$

Here, k_o is the frequency factor, which is a measure of the probability that a molecule having energy E_c will participate in a reaction, and E_c is the apparent activation energy for crystallization. The values of k and n can be determined using the relationship:

$$\ln[-\ln(1-x)] = n \ln k + n \ln(t-\tau) \quad (3)$$

We obtained the JMA plots as shown in Fig. 6c by plotting $\ln[-\ln(1-x)]$ versus $(t-\tau)$ for various temperatures. The data for $10 < x < 90(\%)$ almost shows a straight line behavior, which is coincident with typically linear JMA mode. The values for the Avrami exponents, n, calculated from Fig. 6c using the slope

Table 2. Kinetic parameters of amorphous $Ti_{50}Cu_{20}Ni_{20}Al_{10}$ alloy upon isothermal annealing

Annealing temperature (K)	Incubation time τ (min)	Avrami exponent n (0.1≤x≤0.9)	Reaction rate constant, k
730	5.52	2.53	0.1499
740	1.99	2.60	0.302
750	0.87	2.54	0.63
760	0.23	2.47	1.42

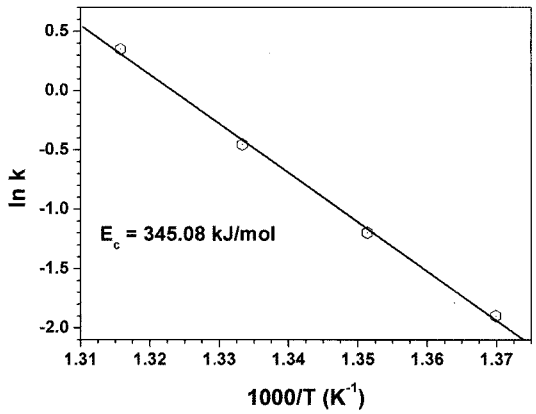

Fig. 7. Arrhenius plot for the isothermal crystallization of $Ti_{50}Cu_{20}Ni_{20}Al_{10}$ alloy.

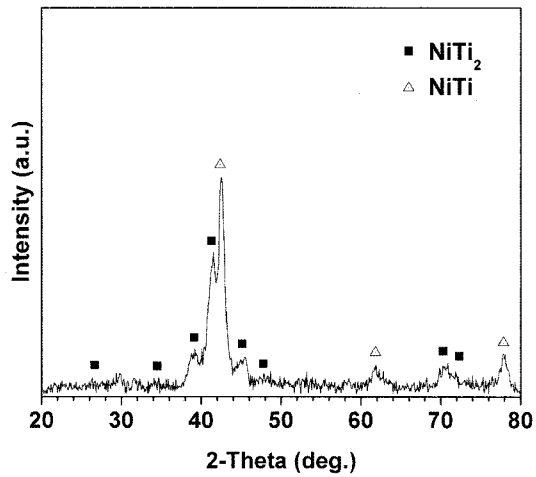

Fig. 8 Crystalline phases of the $Ti_{50}Cu_{20}Ni_{20}Al_{10}$ amorphous powders after heat treatment at 740 K for 45 min.

and intercept of the straight line fitted by the least-squares method are listed in Table 2. The Avrami exponents are close to 2.5, it may be said that the transformation from amorphous to NiTi and $NiTi_2$ intermetallic phases, are diffusion-controlled type at nearly constant nucleation rate [14].

Fig. 7 shows a plot of ln*k* vs. *1/T*, which also yields a straight line. According to Eq. (3), the activation energy is E_c = 345 kJ/mol.

The structural change related to the crystallization event after isothermal at 740 K for 45 min is shown in Fig. 8. The formation of NiTi and $NiTi_2$ intermetallic phases were indexed in the XRD pattern. Our result of Avarami exponent, activation energy and crystalline phase formation under isothermal process is consistent with Vestel *et al.*'s report [16]. He revealed a site-saturation nucleation mechanism with value of n (2.1-2.6) and E_c (~352 kJ/mol) for the formation of crystalline TiNi phase.

4. Conclusions

Fully $Ti_{50}Cu_{20}Ni_{20}Al_{10}$ amorphous powder was successfully synthesized by mechanical alloying after milling of 30 h. The kinetics for crystallization of the amorphous powder was investigated by isothermal DSC analysis. The glass transition and onset crystallization temperatures of the amorphous alloy were 691 and 771K, respectively, with a large SLR of ΔT_x = 80 K. $Ti_{50}Cu_{20}Ni_{20}Al_{10}$ amorphous powder had a wide "temperature-time window" for subsequent consolidation of the powders into bulk materials in the supercooled liquid state. The values of the Avrami exponents were 2.53, 2.60, 2.54, and 2.47 for the isothermal annealing temperatures of 730, 740, 750, and 760 K, respectively. The Avrami exponents are close to 2.5, which correspond to the transformation process of diffusion-controlled type at nearly constant nucleation rate. The activation energy of crystallization process was evaluated according to the Arrhenius equation to be E_c = 345 kJ/mol. The heat treatment at 740K for 45 min leaded to formation of NiTi and $NiTi_2$ intermetallic phases.

Acknowledgments

This work was financially supported by the 2007 Research Fund of the University of Ulsan and Korean Research Foundation (KRF) by the Korea Governments (MOEHARD)(KRF-2006-2110D00221).

References

[1] A. Inoue: Acta. Mater., **48** (2000) 279.

[2] T. Zhang, A. Inoue and T. Masumoto: Mater. Sci. Eng. A, **181/182** (1994) 1423.
[3] A. Inoue, N. Nishiyama and T. Masumoto: Mater. Lett., **19** (1994) 131.
[4] K. Amiya, N. Nishiyama, A. Inoue and T. Masumoto: Mater. Sci. Eng. A, **179/180** (1994) 692.
[5] T. Zhang and A. Inoue: Mater. Trans. JIM, **39** (1998) 1001.
[6] Y. C. Kim, S. Yi, W. T. Kim and D. H. Kim: Mater. Sci. Forum, **360-362** (2001) 67.
[7] I. K. Jeng, Y. Lee, J. S. Chen, R. R. Jeng, C. H. Yeh and C. K. Lin: Intermetal, **10** (2002) 1271.
[8] A. Inoue, T. Zhang, N. Nishiyama, K. Ohba and T. Masumoto: Mater. Trans. JIM, **34** (1993) 1234.
[9] A. W. Weeber and H. Bakker: Physica B, **153** (1988) 93.
[10] L. Schultz: J. Less Common Metals, **145** (1988) 233.
[11] P. P. Choi, J. S. Kim, O. T. H. Nguyen, Y. S. Won: Mater. Sci. Eng. A, **449-451** (2007) 1119.
[12] N. T. H. Oanh, P. P. Choi, J. S. Kim, D. H. Kwond and Y. S. Kwon: Mater. Sci. Forum, **534-536** (2007) 233.
[13] F. Spaepen: Science , **235** (1987) 1010.
[14] R. W. Cahn: "Physical Metallurgy", North Holland Publ. Co., Amsterdam-New York-Oxford, (1977) 525.
[15] M. Avrami: J. Chem. Phys., **7** (1939) 1103.
[16] M. J. Vestel, D. S. Grummon, R. Gronsky and A. P. Pisano: Acta Mater., **51** (2003) 5309.